# Nonlinear electrical impedance of the acoustic stack in cardiac ultrasound probe

**Huynh, Thong[1]; Hoff, Lars[1]; Eggen, Trym Haakon[2]**

[1]Department of Microsystems, University of South-Eastern Norway, Horten, Norway
[2]GE Vingmed Ultrasound AS, Horten, Norway

This is an Accepted Manuscript of an article published by IEEE Online in *2020 IEEE International Ultrasonics Symposium (IUS)* on November 17, 2020, available online: https://doi.org/10.1109/IUS46767.2020.9251312

Huynh, T., Hoff, L., & Eggen, T. (2020, September 7-11). Nonlinear electrical impedance of the acoustic stack in cardiac ultrasound probe [Conference presentation]. 2020 IEEE International Ultrasonics Symposium (IUS). Las Vegas. https://doi.org/10.1109/IUS46767.2020.9251312

# Nonlinear electrical impedance of the acoustic stack in cardiac ultrasound probe

Thong Huynh[1] , Lars Hoff[1] and Trym Eggen[2]
[1]Department of Microsystems, University of South-Eastern Norway, Horten, Norway
[2]GE Vingmed Ultrasound AS, Horten, Norway

***Abstract*— Understanding the nonlinearity in ultrasound probes is important for tissue harmonic imaging, as 2nd harmonic components transmitted from the probe may interfere with harmonics from the tissue and degrade the image quality. The aim of this paper was to identify the main sources of nonlinearity in a medical ultrasound probe. This was done by investigating the capacitive part of its electrical impedance under high excitation voltages, at frequencies well below and well above resonance. We found that when the excitation voltage amplitude was increased from 10 V to 110 V, the free capacitance increased by 50 %, while the clamped capacitance remained unchanged. We also observed an increase with voltage in the loss tangent under free conditions, but not under clamped conditions. We conclude that the nonlinear electrical impedance of the acoustic stack was associated with the mechanical motion and piezoelectric coupling, while contributions from dielectric nonlinearity was negligible.**

## I. Introduction

Tissue harmonic imaging is today the preferred modality in cardiac ultrasound imaging, mainly due to its ability to suppress reverberations [1]. This technique creates images from echoes at the 2nd harmonic of the transmit frequency, generated from nonlinear sound propagation in the tissue [1]–[4]. Nonlinearity in the transmit stage of the ultrasound scanner may interfere with the harmonics from the tissue, diminishing the advantage of harmonic imaging and degrading the image quality. Such nonlinear effects normally increase when the probe is driven by a high voltage, but there are exceptions, e.g. diodes behave nonlinearly at low voltages. The transmit chain of an ultrasound scanner can be divided into two main parts: the electronic transmit circuitry, comprising electrical excitation sources and tuning, and the ultrasound transducer. The transducer consists of an acoustic stack with a piezoelectric layer sandwiched between acoustic matching and backing layers, with an acoustic lens in front. In a previous study [5] we found that harmonics in the transmit stage were predominantly generated in the ultrasound transducer, i.e. in the acoustic stack. The present study goes one step further to identify the main sources of nonlinearity inside the stack. This is done by investigating how the capacitive part of the transducer impedance changes at high excitation voltages, measured at frequencies well below and well above the transducer resonances.

This work was supported by the Research Council of Norway, project number 237887.

Nonlinearities in the transducer may relate to its structural design, e.g. CMUTs have an intrinsic nonlinear relation between membrane vibration and applied voltage. For transducers using a bulk piezoelectric, this relation is commonly assumed to be linear, but high excitation levels may create nonlinearities also in these devices. In the passive materials that constitute the backing and matching layers, nonlinearities may occur at high strain and stress levels, seen as a nonlinear stress-strain relation [6]. In the piezoelectric material, a nonlinear response can be explained by nonlinear mechanisms on the microscopic level. Several studies on nonlinearity in the piezoelectric attempt to separate the nonlinearity into 3 main sources using the corresponding coefficients in the piezoelectric constitutive equations: elastic, electric and piezoelectric [7]–[11]. Perrin et. al observed analogies between the dielectric and piezoelectric nonlinearities, and suggested they are controlled by the same 90° domain wall translation mechanism [12]. Other researches showed that nonlinearity in electric, elastic and piezoelectric material coefficients have a common origin, identified as the movement of the domain walls [8], [13], [14]. However, distinguishing the nonlinearity into elastic, dielectric and piezoelectric is challenging, and will depend on the chosen form of the piezoelectric constitutive equations.

The aim of this paper was to investigate and identify mechanisms contributing to nonlinearity in the acoustic stack. This was done by measuring the capacitance at frequencies well below and above the resonances, and study how they varied with excitation voltage.

## II. Method

### A. Theory

A common lumped circuit model for an electro-acoustic transducer is the Butterworth Van-Dyke (BVD) model [15] shown in Fig. 1. The right branch of the circuit ($C_m$, $R_m$, $L_m$) is the motional branch, with electrical equivalents of the mechanical elements, while $C_0$ is the clamped capacitance. At low frequencies, the capacitor $C_m$ dominates the impedance in the motional branch, and the impedance is capacitive with the *free capacitance* $C_f = C_0 + C_m$. At frequencies well above resonance, the mechanical inductor $L_m$ blocks the mechanical branch and the impedance will also be capacitive, now with *clamped capacitance* $C_0$. The physical interpretation of this is that the transducer is free to move at low frequencies, while inertia blocks movements at high frequencies.

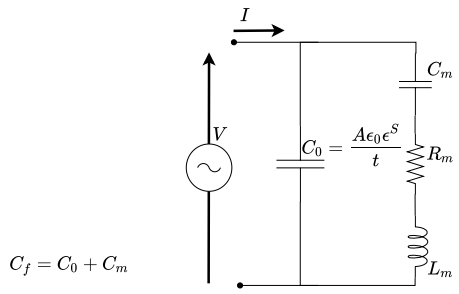


Fig. 1. Butterworth Van-Dyke (BVD) model for the electro-acoustic transducer. The free capacitance $C_f$ measured at low frequency is the sum of the clamped capacitance $C_0$ and the capacitance in the motional branch $C_m$. At high frequency, the impedance approaches $C_0$.

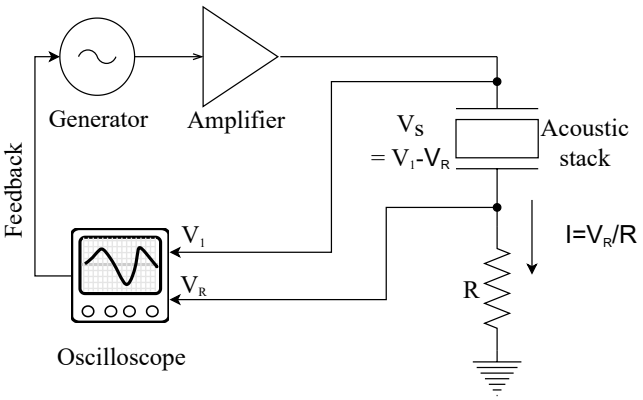


Fig. 2. Schematic illustration of the experimental setup for measuring electrical impedance at different voltage levels. The voltage $V_S$ over and current $I$ through the stack were calculated by measuring $V_1$ and $V_R$ in the schematic. The impedances were obtained by taking the ratio of voltage to current at the center frequency of the driving voltage pulse, and the capacitances were calculated from the imaginary part of the impedances.

The free and clamped capacitances of a transducer can be approximated from the imaginary part of the transducer impedance measured at frequencies well below and well above the main resonance. $C_0$ is proportional to the clamped electrical permittivity, while $C_m$ depends on the piezoelectric constant and mechanical stiffness. Characterization of these capacitances can provide insight into the mechanisms behind the nonlinearity in the acoustic stack: Measurements on how the free $C_f$ and clamped $C_0$ capacitances vary as function of excitation voltage may make it possible to identify the main nonlinear mechanisms behind the transmitted 2nd harmonics.

### *B. Nonlinear electric impedance of the acoustic stack*

When a transducer is driven at frequency $f_0$, a nonlinear impedance can lead to harmonic terms in both voltage and current. In this case, the total current $I$ through and voltage $V$ over the acoustic stack will contain both the driving angular frequency $\omega_0 = 2\pi f_0$ and its harmonics,

$$V = \sum_{n=0}^{\infty} \hat{V}_n e^{jn\omega_0 t} \qquad I = \sum_{n=0}^{\infty} \hat{I}_n e^{jn\omega_0 t}\,, \tag{1}$$

where $n$ is an integer number representing the harmonics, and $\hat{V}_n$ and $\hat{I}_n$ are complex numbers giving amplitude and phase of the harmonic terms in voltage and current. With harmonic terms, the definition of a frequency dependent impedance $Z(\omega)$ is not uniquely defined. We have chosen to look at the ratio of voltage $V(\omega)$ to current $I(\omega)$ at the fundamental frequency $\omega_0$, and define the electrical impedance $Z(\omega_0)$ at driving angular frequency $\omega_0$ by

$$Z(\omega_0) = \frac{\hat{V}_1(\omega_0)}{\hat{I}_1(\omega_0)}\,. \tag{2}$$

The capacitance $C(\omega_0)$at frequency $\omega_0$ is calculated from the imaginary part of the impedance $\mathrm{Im}\{Z_0(\omega_0)\}$ as

$$C(\omega_0) = -\frac{\mathrm{Im}\{Z_0(\omega_0)\}}{\omega_0}\,. \tag{3}$$

### *C. Measurement setup*

The measurement setup for measuring impedance is illustrated in Fig. 2. The transducer investigated in this this paper was one element in a 1D array designed for adult cardiac imaging, having a bandwidth from 1.4 to 4.6 MHz.

The transducer element, referred to as the acoustic stack, was driven by a 14-bit arbitrary waveform generator (PicoScope 5244B, Pico Technology) connected to a power amplifier (E&I 2100L, Electronics& Innovation, Ltd). The amplifier was connected directly to the acoustic stack, without any electric tuning network. The current through the stack was found by adding a resistor in series and measuring the voltage $V_R$ over this resistor. The resistor value 10 Ω was much smaller than the stack impedance, so grounding conditions were not violated. The power amplifier was designed to work with a 50 Ω load, and its output voltage depends on the load impedance. The impedance of the acoustic stack varies with frequency, causing the output voltage from the amplifier to change with frequency for a given input voltage. This was compensated for by recording the voltage over the stack by the oscilloscope (PicoScope 5244B) and using this as feedback to the generator, maintaining a constant voltage over the stack when measuring at low and high frequencies.

The acoustic stack was driven by 5-cycle Gaussian enveloped sine-wave bursts with center frequency either $f_{LF}$=0.1 MHz or $f_{HF}$=10 MHz. Voltage $v(t)$ and current $i(t)$ over the acoustic stack were measured as function of time $t$, and transformed into the frequency domain using fast Fourier transform (FFT) without windowing. At each frequency, the impedance was calculated according to (2). The measurements were repeated for 10 MHz pulses having the same pulse duration as the 0.1 MHz pulses, enclosed in the same Gaussian envelope, i.e. 500-cycle pulses. This was done to compare pulses of the same total pulse energy, in contrast to pulses with the same number of cycles.

Measurements were done first at the low frequency 0.1 MHz then at the high frequency 10 MHz. At each frequency, the voltage amplitude was increased from 10 V to 110 V. The measurement procedure was repeated with the acoustic stack replaced by a passive load of similar electrical impedance, implemented as the BVD-model in

Fig. 1. Component values used in the circuit were $C_0$=120 pF, $C_m$=50 pF, $R_m$=470 Ω, and $L_m$=60 µH. The impedance curves of the stack and the passive load were also measured using a vector network analyzer (R&S ZVL, Rohde & Schwarz, Germany) to verify our setup against a reference instrument.

## III. Results

### A. Capacitances

Fig. 3 shows how the capacitance depends on excitation voltage at frequencies $f_{LF}$=0.1 MHz and $f_{HF}$=10 MHz. At the low frequency, 0.1 MHz, the capacitance increased from 153 pF to 224 pF, approximately 50 %, when the excitation voltage amplitude was increased from 10 V to 110 V. No such variation was seen for the capacitance at 10 MHz, showing less than 2 % variation over the voltage range. Repeating the measurements with high frequency pulses scaled to the same pulse duration as the low frequency pulses gave $C_{HF}$=(90 ± 2) pF at $f_{HF}$=10 MHz, with variation less than 3 % over the voltage range.

When the measurements were repeated on the passive load in Fig. 1, the capacitance was measured to $C_{LF}$=(172.0 ± 0.2) pF at 0.1 MHz and $C_{HF}$=(119 ± 2) pF at 10 MHz. The variation over the voltage range was less than 2 % at both frequencies.

### B. Loss tangent

The real and imaginary part of the measured impedances $Z(\omega_0)$ at frequencies $f_{LF}$=0.1 MHz and $f_{HF}$=10 MHz are plotted Fig. 5, showing how the loss tangent depends on excitation voltage. At the lowest voltage, $V_S$=10 V, the impedances at both the low and high frequency show a phase lower than −83°, i.e. the impedances are almost purely capacitive. As the driving voltage amplitude increases, both the imaginary and the real part of the impedance increase at the low frequency. This corresponds to an increase in loss tangent. In contrast to this, at the high frequency, the loss tangent did not change with increasing voltage.

## IV. Discussion

### A. Interpretation of capacitance measurements

The capacitance measurements in Fig. 3 indicate that the free capacitance $C_f$ increases with excitation voltage, while no such dependence is seen in the clamped capacitance $C_0$. The clamped capacitance $C_0$ corresponds to no motion, and is given by the clamped electrical permittivity only. The free capacitance $C_f$ includes additional contributions from mechanical motion and piezoelectric coupling. The result is interpreted as that the observed nonlinearity is linked to mechanical motion and piezoelectric coupling, while nonlinear electrical permittivity is negligible in comparison. The plots of $Z(\omega_0)$ in the complex plane (Fig. 5) display another manifestation of nonlinearity seen under free conditions, but not under clamped conditions: The increase in loss tangent as driving voltage increases. This corresponds to the results of Albareda et al. who observed a similar variation for the motional impedance of a piezoelectric near resonance [16].

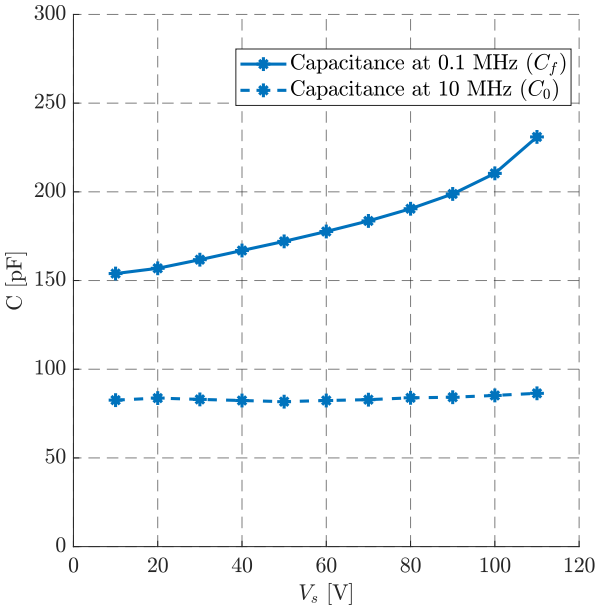


Fig. 3. Variation in acoustic stack capacitance as function of driving voltage amplitude, measured at low (0.1 MHz) and high (10 MHz) frequency. As the voltage increases, the stack capacitance measured at low frequency ($C_f$) increase while the capacitance at high frequency ($C_0$) remains unchanged.

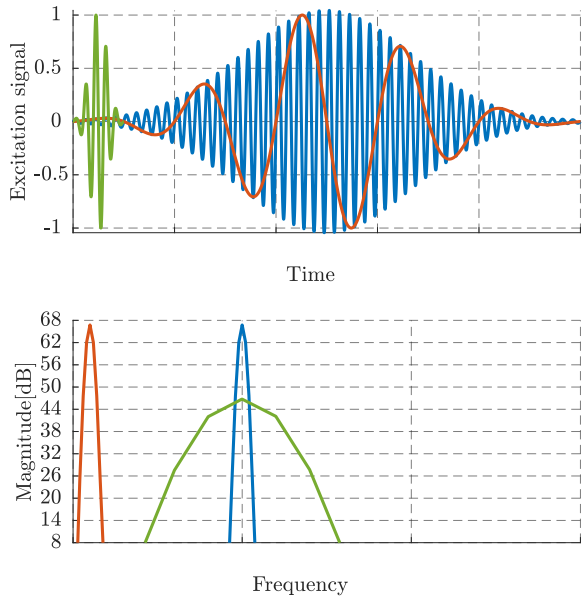


Fig. 4. Schematic (not to scale) illustration of excitation pulses and their spectra. With the same number of periods, 5 cycles, the low frequency pulse (red) is longer and contains more energy than the high frequency pulse (green). Alternatively, the 5-cycle low frequency pulse can be compared to a high frequency pulse with the same duration and envelope (blue).

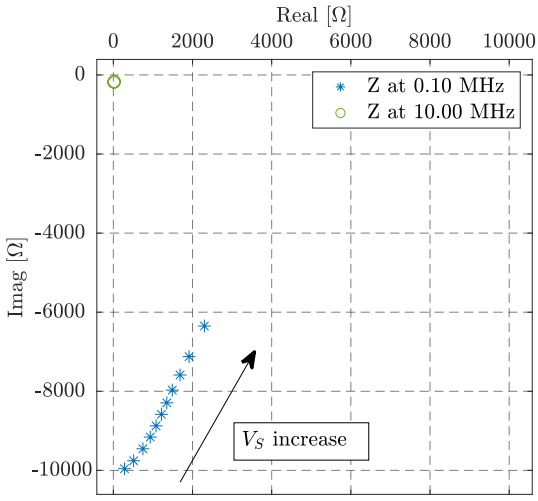


Fig. 5. Real and imaginary parts of the impedance in the acoustic stack, measured at low (0.1 MHz) and high (10 MHz) frequencies.

### B. Parasitic capacitances

Parasitic capacitances in e.g. cables and connections may influence the results. As long as these parasitic capacitances are independent of voltage, they will cause a constant shift of the curves in Fig. 3, and will not alter the conclusions of this study. This is further confirmed by the results when the acoustic stack was replaced by the passive load in Fig. 1. These measurements showed negligible variation in the capacitances when the voltage was changed, demonstrating that the variation with voltage is due to the acoustic stack and not other parts of the system.

### C. Effect of pulse energy

Comparing pulses of different frequencies is not unique. When the same number of cycles is used, the relative bandwidths are equal, but the energy in the low frequency pulse is larger than in the high frequency pulse. The phenomenon is illustrated in Fig. 4, comparing two pulses at center frequency 10 MHz with one at 0.1 MHz. One 10 MHz pulse has the same number of cycles as the 0.1 MHz pulse, the other has the same pulse duration and envelope.

If nonlinearities depend on energy and not on amplitude, this may explain a stronger nonlinearity at low frequency where a higher pulse energy was used. This was tested by repeating the experiment with the high frequency pulses having the same pulse duration and envelope, i.e. the same energy, as the low frequency pulses. The result of this experiment was identical to the results for the shorter pulses, both giving less than 3 % variation over the voltage range tested. This indicates that the observed nonlinear effect depends on voltage amplitude and not on pulse energy.

## V. Conclusion

Nonlinearities in clinical ultrasound probe was investigated by comparing the capacitance at two frequencies. The low frequency, well below resonance, corresponds to free conditions while the high frequency, well above resonance, corresponds to clamped conditions. When the driving voltage amplitude was increased from 10 V to 110 V, we observed a 50 % increase in the free capacitance, while no change in clamped capacitance was seen over the same voltage range. The loss tangent was found to increase with driving voltage under free conditions, while it was independent of voltage under clamped conditions.

We conclude that nonlinearity in a piezoelectric transducer is connected to mechanical motion and piezoelectric coupling, while the nonlinearity from dielectric properties is negligible.

## References


[1] M. Averkiou, "Tissue harmonic imaging," in *2000 IEEE Ultrasonics Symposium. Proceedings. An International Symposium (Cat. No.00CH37121)*, vol. 2, pp. 1563–1572, IEEE, 2000.

[2] F. Tranquart, N. Grenier, V. Eder, and L. Pourcelot, "Clinical use of ultrasound tissue harmonic imaging," *Ultrasound in Medicine & Biology*, vol. 25, pp. 889–894, 7 1999.

[3] T. S. Desser and R. Jeffrey, "Tissue harmonic imaging techniques: Physical principles and clinical applications," *Seminars in Ultrasound, CT and MRI*, vol. 22, pp. 1–10, 2 2001.

[4] B. Ward, A. C. Baker, and V. F. Humphrey, "Nonlinear propagation applied to the improvement of resolution in diagnostic medical ultrasound," *J Acoust Soc Am.*, vol. 101, pp. 143–154, 1 1997.

[5] T. Huynh, L. Hoff, and T. Eggen, "Sources of 2nd Harmonic Generation in a Medical Ultrasound Probe," in *IEEE International Ultrasonics Symposium, IUS*, vol. 2018-Octob, 2018.

[6] W. C. Orthwein, "A nonlinear stress-strain relation," *International Journal of Solids and Structures*, vol. 4, pp. 371–382, 3 1968.

[7] D. Kobor, A. Hajjaji, J. E. Garcia, R. Perez, A. Albareda, L. Lebrun, D. Guyomar, D. Kobor, A. Hajjaji, J. E. Garcia, R. Perez, A. Albareda, L. Lebrun, and D. Guyomar, "Dielectric and Mechanical Nonlinear Behavior of Mn Doped PMN-35PT Ceramics," *Journal of Modern Physics*, vol. 01, pp. 211–216, 10 2010.

[8] P. Gonnard, "Investigation on dielectric, mechanical and piezoelectric non-linearities in piezoceramics through a new equivalent circuit," in *ISAF 2000. Proceedings of the 2000 12th IEEE International Symposium on Applications of Ferroelectrics (IEEE Cat. No.00CH37076)*, vol. 2, pp. 691–694, IEEE, 2000.

[9] A. Albareda, R. Pérez, J.-H. Kayombo, E. Minguella, J.-A. Casals, and F. Montero de Espinosa, "Nonlinear mechanical behavior of piezocomposites for ultrasonic transducers," *Ultrasonics*, vol. 38, pp. 151–155, 3 2000.

[10] D. Kobor, A. Albareda, R. Perez, J. Garcia, L. Lebrun, and D. Guyomar, "Dielectric and mechanical nonlinearities of lang001rang oriented pure and doped single crystals of PZN-4.5PT," *Journal of Physics D: Applied Physics*, vol. 38, pp. 2258–2264, 7 2005.

[11] D. Parenthoine, L. Haumesser, F. Meulen, M. Lethiecq, and L.-P. Tran-Huu-Hue, "Nonlinear constant evaluation in a piezoelectric rod from analysis of second harmonic generation," *IEEE Trans Ultrason Ferroelectr Freq Control*, vol. 56, pp. 167–174, 1 2009.

[12] V. Perrin, M. Troccaz, and P. Gonnard, "Non Linear Behavior of the Permittivity and of the Piezoelectric Strain Constant Under High Electric Field Drive," *Journal of Electroceramics*, vol. 4, no. 1, pp. 189–194, 2000.

[13] D. Damjanovic, "Stress and frequency dependence of the direct piezoelectric effect in ferroelectric ceramics," *Journal of Applied Physics*, vol. 82, pp. 1788–1797, 8 1997.

[14] P. M. Chaplya and G. P. Carman, "Dielectric and piezoelectric response of lead zirconate–lead titanate at high electric and mechanical loads in terms of non-180° domain wall motion," *Journal of Applied Physics*, vol. 90, pp. 5278–5286, 11 2001.

[15] K. Van Dyke, "The Piezo-Electric Resonator and Its Equivalent Network," *Proceedings of the IRE*, vol. 16, pp. 742–764, 6 1928.

[16] A. Albareda, P. Gonnard, V. Perrin, R. Briot, and D. Guyomar, "Characterization of the mechanical nonlinear behavior of piezoelectric ceramics," *IEEE Trans Ultrason Ferroelectr Freq Control*, vol. 47, no. 4, pp. 844–853, 2000.